Mon. Not. R. Astron. Soc. **000**, 000–000 (1996) Printed 1 February 2008

The X-ray spectral properties of X-ray selected AGN : ROSAT spectra of EMSS AGN

P.Ciliegi,[1,2] and T. Maccacaro,[2]

1. Istituto di Radioastronomia del CNR - Via P. Gobetti 101, 40129 Bologna, Italy

2. Osservatorio Astronomico di Brera, Via Brera 28, 20121 Milano, Italy

Accepted May 1996. Submitted December 1995

ABSTRACT

Using a sample of 63 AGNs extracted from the *Einstein* Extended Medium Sensitivity Survey (EMSS), we study the X-ray spectral properties of X-ray selected AGN in the 0.1−2.4 keV ROSAT band. These objects are all the EMSS AGN detected with more than 300 net counts in ROSAT PSPC images available from the public archive (as of May 31, 1995). A Kolmogorov-Smirnov test on the redshift and luminosity distributions shows that this subsample is representative of the whole EMSS sample.

For the 21 sources detected with less than 600 net counts we characterize the spectrum only with the hardness ratio technique. For the other 42 sources we obtain a detailed spectral analysis fitting the data with two different power-law models: one with N_H fixed at the Galactic value and one with N_H as a free parameter. Eight sources ($\sim$ 20 per cent) show a significant deviation from a power-law absorbed by Galactic N_H, indicating soft excess (five sources) or excess absorption (three sources). These eight sources are analyzed and discussed separately and are excluded from the sample used to study the mean X-ray spectral properties of the EMSS sources.

A Maximum-Likelihood analysis is used to find the mean power-law spectral index $< \alpha_p >$ and the intrinsic dispersion σ_p. We find $< \alpha_p >$=1.42 with σ_p=0.44. This value is significantly steeper ($\Delta\alpha \sim$0.4) than the mean *Einstein*/IPC spectral index obtained applying the ML analysis on the whole sample of EMSS AGN. This result shows that the soft excess already noted in optically selected AGN is present also in X-ray selected AGN. The relatively high value obtained for the intrinsic dispersion confirms that in the soft band AGN are characterized by a variety of spectral indices and the increase with respect to the results obtained from the analysis of Einstein data ($\Delta\sigma_p \sim$0.16) suggests a further broadening of the spectral index distribution as one moves to softer energies. A comparison between the mean spectral index of Radio-quiet and Radio-loud subsamples shows that the mean index of the RL sample is flatter than that of RQ, both in the IPC ($\Delta\alpha \sim$0.3) and in the PSPC ($\Delta\alpha \sim$0.4) data. This suggests that the additional X-ray component in RL AGN dominates the X-ray emission of RL AGN over almost two decades of energy ($\sim$0.1−10 keV). Finally, we find no significant correlation between the spectral index α_x and other physical parameters such redshift, optical and X-ray luminosity.

Key words: galaxies:active − galaxies:nuclei − quasars:general − X-ray: galaxies

1 INTRODUCTION

The X-ray spectra of AGN have been studied extensively over the last decade using a variety of instruments aboard different satellites (see, among others, Petre et al. 1984, Reichert et al. 1985, Wilkes and Elvis 1987, Canizares and White 1989, Turner and Pounds 1989, Comastri et al. 1992, Williams et al. 1992, see also Malaguti et al. (1994) for a catalog of all the X-ray spectra of AGN published from the early 70's to the end of 1992).

These studies indicate that the X-ray emission above 1-2 keV is well described by a power-law with a spectral slope $\alpha_x \sim$0.5 ($f_\nu \propto \nu^{-\alpha}$) for radio-loud (RL) objects and $\alpha_x \sim$1.0 for radio-quiet (RQ) objects. Below 1 keV an excess emission relative to the flux predicted by an extrapolation of the hard X-ray power-law is observed (Wilkes and Elvis

1987, Comastri et al. 1992). Most of the objects studied are among the brightest in the X-ray band ($f_x \geq 1 \times 10^{-12}$ erg cm^{-2} s^{-1} 0.3−3.5 keV) and do not form a complete sample. Although the *Einstein* satellite has produced large samples of X-ray selected AGN, the information available on their X-ray spectral properties is limited by the poor energy resolution of the IPC and by the limited statistics of the detected sources. For the *Einstein* Extended Medium Sensitivity Survey AGN sample (EMSS: Gioia et al. 1990, Stocke et al. 1991, Maccacaro et al. 1994), for instance, only the few brightest sources (*e.g.* MKN 766, MKN 205, MKN 1310, PG1416-12, PG1426+015, MKN 877) could be analyzed in some detail (see Halpern 1981, Elvis et al. 1986, Wilkes and Elvis 1987, Kruper et al. 1990). Since the majority of the EMSS sources had less than 150 net counts only a statistical analysis of the *average* spectral properties was possible, by means of the analysis of their Hardness Ratio (HR).

Using the HR technique, Maccacaro et al. (1988) reported an average energy spectral index $< \alpha_x >$=1.03 with an intrinsic dispersion σ=0.36 for the EMSS AGN sample.

The better sensitivity, energy resolution (E/ΔE=2.4(E/1 keV)$^{1/2}$ FWHM) and spatial resolution of the PSPC detector aboard the ROSAT satellite (Trümper, 1983) allow us to improve upon the previous study and to extend the spectral analysis of representative samples of faint AGN ($f_x \simeq 1 \times 10^{-13}$ erg cm^{-2} s^{-1}) to slightly softer energies.

Recently, Ciliegi et al. (1996) have reported a detailed X-ray spectral analysis in the 0.1−2.4 keV band of a complete sample of X-ray selected AGN. Using the 80 AGN (68 QSO and 12 narrow emission line galaxies, NLXGs) in the Cambridge-Cambridge ROSAT Serendipity Survey (CRSS, Boyle et al. 1995) they found that a single power-law plus Galactic absorption yields a good representation of the X-ray spectra for almost all the sources, with a mean energy spectral index $< \alpha_x >= 1.32$ (dispersion $\sigma = 0.33$) for the quasar sample and $< \alpha_x >= 1.30$ ($\sigma = 0.49$) for the NLXG sample. Puchnarewicz et al. (1996) have also analyzed the spectral properties of X-ray selected AGN using a sample of 108 objects in the ROSAT International X-ray/Optical Survey (RIXOS). They found an average spectral index $< \alpha_x >$=1.07 ($\sigma = 0.63$), marginally flatter than the CRSS average spectral index. Finally Laor et al. (1994) and Walter and Fink (1993) have analyzed optically selected samples of quasar obtaining a mean ROSAT spectral index of $\alpha \simeq$1.50.

In this paper we report the soft X-ray spectral analysis of all the EMSS AGN detected with more than 300 net counts in the ROSAT/PSPC public (as of May 31, 1995) observations. In section 2 we define the sub-sample of the EMSS AGN used, while in section 3 we describe the method of analysis. We report and discuss the results in section 4 and 5 respectively, while in section 6 the conclusions and a summary are presented. Throughout the paper a Hubble constant of $H_0 = 50\,\mathrm{km\,s^{-1}\,Mpc^{-1}}$ and a deceleration parameter $q_0 = 0$ are assumed.

2 THE SAMPLE

We searched in the ROSAT archive for ROSAT (PSPC) images containing pointed or "serendipitous" observations of EMSS AGN. The first selection criterion used is an off-axis angle θ (the distance between the source and the center of the PSPC field) smaller than 50 arcmin. We find data for 203 different EMSS AGN. Because our aim is a detailed study of the X-ray spectral properties, we then selected only those sources detected with more than 300 measured net counts. For sources observed more than once, we retain only the observation where the object is detected with the highest number of net counts. We find 63 EMSS AGN satisfying the above criteria; they are listed in Table 1 which is organized as follows: source name, followed by redshift, the two point spectral index between radio and optical band (α_{ro}, from Stocke et al. 1991), the extraction radius r (arcmin) calculated as described in section 3, the off-axis angle θ (arcmin), the net counts detected in the 0.1−2.4 keV band within the r radius circle with the relative error computed as the square root of the total (source + background) observed counts, and the sequence number of the ROSAT observations. Sources for which "normalized" net counts have been computed (see Section 3 for details) are indicated with an asterisk.

Five of these 63 objects are radio-loud objects on the basis of the standard radio to optical spectral index criterion ($\alpha_{ro} \geq$0.35).

A Kolmogorov-Smirnov (KS) test shows that the redshift, X-ray and optical luminosity distributions of the 63 EMSS AGN discussed in the present paper are not significantly different (at a confidence level greater than 90 per cent) from the distributions of the whole EMSS AGN sample . Moreover we have checked whether the requirement that the sources have more than 300 net counts could introduce a bias in the spectral index distribution due to the fact that steeper spectrum sources could have higher ROSAT count rates. We have searched for a possible correlation between net counts and spectral indices but we found no evidence for it.

We are therefore confident that, although in our analysis we used only $\sim$ 15 per cent of the EMSS AGN, the results obtained are representative of the whole sample. We can then compare the mean ROSAT/PSPC spectral properties of the subsample of 63 objects with the mean *Einstein*/IPC spectral properties of the whole sample, taking advantage of the large size of the latter.

3 DATA ANALYSIS

For each source we fit the X-ray image with a two-dimensional gaussian to determine its centroid. Subsequently we extract the total counts in the $0.1 - 2.4\,\mathrm{keV}$ band using a circle centered on the source centroid. To optimize the signal to noise ratio the extraction radius r is chosen to be the distance from the centroid at which the radial profile of the point source meets the background level. All the extraction radii lay in the range $2.0' \leq r \leq 5.0'$. The background counts are estimated in an annulus centered on the source with inner radius $r + 1'$ and outer radius $r + 3'$. When other sources are detected within the background region, they are removed using a cutting circle with a radius chosen to contain at least 95 per cent of

the source counts (Turner and George 1992). For the 11 sources detected near other sources or near the window support structure, an azimuthal sector centered on the source position is excluded from the circle used for the counts extraction (and from the annulus used for the background determination) to avoid contamination or shadowing. The net counts thus obtained are used for the spectral analysis. The X-ray flux of these sources, however, is determined normalizing the net counts to a full circle, assuming that the source net counts are azimuthally uniformly distributed. Thus, for example, when we exclude a 90° azimuthal sector, the normalized net counts (and relative error) are obtained multiplying the measured counts (and error) by 360/(360-90). For the four sources (MS0439.7−4319, MS0919.3+5133, MS1059.0+7302, MS1408.1+2617) detected near the window support structure we included a systematic error of 10% in the X-ray flux by adding it in quadrature to the statistical error. Sources for which normalized net counts have been computed are indicated in Table 1.

For all sources we have computed the energy spectral index α_x of the power-law using the hardness ratio HR and fixing N_H at the Galactic value. The hardness ratio HR is defined as HR = (H−S)/(H+S) where S is the number of net counts detected in the 0.11−0.43 keV band and H is the number of net counts detected in the 0.5−2.02 keV band (see Appendix A in Ciliegi et al. 1996 for a full description of the ROSAT hardness ratio technique). Following Hasinger (1992), before computing the hardness ratio, we have corrected the net counts of each source for the energy dependence of the Point Spread Function (PSF). Of the 63 sources, 42 are detected with more than 600 net counts. For these sources a more detailed spectral analysis is possible. We have thus considered 31 of the 34 energy channels from the MPE Standard Analysis Software System (SASS) pipeline processing excluding the first two channels (< 0.1 keV) and the last channel (> 2.4 keV) because the response of the instrument is not well-defined at the extremes of the energy range. The spectrum is then binned to obtain at least 20 net counts and a signal to noise ratio $S/N \geq 3$ in each bin so that the χ^2 statistic could be applied. Finally we make two different power-law fits: (1) with N_H fixed at the Galactic value and (2) with N_H as free parameter. Model fits are carried out using the XSPEC software package, and the best fit model parameters are obtained by χ^2 minimization. Following Fiore et al. (1994), we have used the 1992 March response matrix for observations made before October 1991 and the 1993 January response matrix for observations made after October 1991.

4 RESULTS

The results of the spectral fits are given in Table 2. For each source we report the results of the hardness ratio analysis (columns 2 and 3) and of the detailed spectral analysis (columns 4 - 9). The table is organized as follows:

Column 1: Source name. Radio-loud AGN are indicated with "R".

Column 2: Hardness Ratio (HR).

Column 3: Energy spectral index α_{HR} obtained from the HR, fixing $N_H = N_{H_{\rm Gal}}$.

Column 4: Best fitting spectral slope α_x for fit 1 (first row) and for fit 2 (second row).

Column 5: $N_{H_{\rm Gal}}$ used for fit 1 (first row) and the best fitting N_H for fit 2 (second row).

Column 6: χ^2 of the fit ($\chi^2_{\rm FIT}$) and the number of degrees of freedom (dof) for fit 1 (first row) and fit 2 (second row).

Column 7: Probability for $\chi^2 \geq \chi^2_{\rm FIT}$.

Column 8: F-test probability (Bevington and Robinson 1992) that the reduction in $\chi^2_{\rm FIT}$ with the addition of N_H as a free parameter is not statistically significant ($P(F > F_{\rm FIT})$).

Column 9: X-ray flux in the 0.1−2.4 keV band obtained using the fit 1 parameters or, for sources with less than 600 net counts, using α_{HR} and Galactic N_H. Flux errors are computed from photon-counting statistics only (*i.e.* without taking into account the error on the spectral slope and on N_H).

The errors represent the 68 per cent confidence intervals for a single interesting parameter when N_H is fixed, and for two interesting parameters when both the X-ray energy spectral index α_x and N_H are free to vary.

A comparison of fit 1 and 2 allows us to determine whether there is evidence for a significant intrinsic excess absorption or excess emission relative to a single power law model plus Galactic absorption. As shown in Table 2, in eight of the 42 objects for which we have enough net counts to allow a spectral fit, there are significant deviations from a simple power-law plus Galactic absorption (i.e. $P(F > F_{\rm FIT}) < 0.01$). These eight sources, that will be separately discussed in § 5.1, represent about 20 per cent of the sources with more than 600 net counts.

Finally, we have used these 42 sources to test the reliability of the hardness ratio technique by comparing the spectral indices α_{HR} derived from the hardness ratio with those derived from the detailed spectral analysis (fit 1: N_H fixed at the Galactic value). The result is illustrated in Figure 1. The slope derived by the two method are very well correlated through a wide range of values ($\alpha_x \sim 0.4 - 2.2$). For $\alpha_x > 2.2$ (3 objects) the slopes obtained from the hardness ratio are lower ($\Delta\alpha \sim 0.2$) than those obtained from the detailed spectral analysis. This same difference was evident also in the results of the X-ray spectral analysis of the CRSS AGN sample (Ciliegi et al. 1996). Since all the EMSS AGNs analyzed solely with the HR show an energy spectral index α_x <2.1 (see Table 2) we are confident that can safely combine the results obtained with the two techniques. Of course one should keep in mind that the hardness ratio technique is not able to recognize those sources showing a significant deviation from a power-law model plus Galactic absorption, since its application rests on the assumption of the knowledge of the spectral form. However, on the basis of the results obtained from the detailed analysis of the 42 sources detected with more than 600 net counts we expect that this assumption (*i.e.* X-ray spectra well fitted by a simple power-law plus Galactic absorption) may not be appropriate only for ∼20 per cent of the 21 sources analyzed with this technique (*i.e.* ∼ 4 sources).

We have therefore removed the 8 sources that show significant deviations from a single power-law model plus Galactic absorption to obtain a sample of 55 AGN which we use in the following. Given the small number of objects for

which the HR results may be unreliable (<8 per cent of the whole sample of 55 objects) the results obtained should not be strongly affected by their possible inclusion.

5 DISCUSSION

5.1 *5.1 Sources with a significant deviation from a simple power-law plus Galactic absorption*

As discussed above, eight sources show a significant deviation from a simple power-law fit plus Galactic absorption. Five of these sources show a best fit value of N_H lower than the Galactic value, indicating an excess of soft emission relative to a single power-law fit with N_H=$N_{H_{Gal}}$, while the other three sources show excess absorption (N_H >$N_{H_{Gal}}$). For only two of these eight sources (MS1215.9+3005 and MS1747.2+6837) there are ROSAT/PSPC spectra already published in the literature (Molendi and Maccacaro 1994, Brandt et al. 1994). For the other six sources we plot in Figure 2 a two dimensional contour plot for a single power-law model with spectral slope α_x and equivalent hydrogen absorbing column density N_H. Below we briefly discuss each of these sources in turn.

MS0104.2+3153 This X-ray sources is a QSO-Galaxy pair discovered as a serendipitous source in the EMSS. Based upon the IPC data (52 net counts, Gioia et al. 1990) the true identity of MS0104.2+3153 was ambiguous due to the presence in the error circle ($\sim 40''$) of a radio-quiet broad absorption line (BAL) QSO (z=2.027) only $10''$ away from a giant elliptical galaxy (z=0.111) at the center of a compact group of galaxies (Stocke et al. 1984). Successively, this source was observed with the Channel Multiplier Array (CMA) aboard the EXOSAT satellite (Gioia et al. 1986). Since no X-ray source was apparent in the deep (160 ksec) EXOSAT observation, Gioia et al. (1986) concluded that the X-ray source is variable and thus that the QSO is the strongest candidate for the optical identification of MS0104.2+3153 excluding any contribution to the X-ray flux from the giant elliptical galaxy or from the cluster of galaxy. Moreover, Gioia et al. (1986) concluded that the EXOSAT CMA data implied a substantial decrease in the X-ray luminosity of this object, unless its soft X-ray spectrum is unusually and extremely flat (α_x <0.2) or this object exhibits a significant amount of intrinsic absorption ($N_H > 2\times10^{21}$ cm^{-2}; quite possible for a BAL QSO).

The ROSAT observation allow us to study in more detail the X-ray emission from this source. Unfortunately, in spite of the improved spatial resolution of the ROSAT/PSPC detector, we are not yet able to confirm, on positional ground, the optical identification of this source. As shown in Figure 2a (see also Table 2) this source has a best fit N_H value larger than the Galactic value at the 99 per cent confidence level. We fit the absorption excess modelling the data with a power-law plus Galactic absorption plus a second absorption component. We make two different fits, with the additional absorption component fixed at the redshift of the cluster (z=0.111, fit A) and at the redshift of the QSO (z=2.027, fit B). In table 3 we report the results of these spectral models. The PSPC cannot constrain the redshift of the absorbing material, both models give, in fact, a good fit of the data (see Table 3).

The spectral results (models A e B, Table 3) show that the X-ray spectrum of this source is characterized by a very steep spectral index ($\alpha_x > 2.9$) and by a strong excess absorption relative to the Galactic value ($N_H > 4 \times 10^{21}$). Therefore, the non detection with the EXOSAT CMA can not be attributed to an unusually and extremely flat spectrum. However the possibility that the non detection is not due to an X-ray flux variability but to a significant amount of intrinsic absorption can not be excluded.

In conclusion, the ROSAT observation of MS0104.2+3153 does not allow us to obtain a definite identification of the X-ray source.

MS0132.5−4151 This source shows a best fit value of N_H lower than the Galactic value at the 99 per cent confidence level (see Figure 2b). We parameterized this soft excess fitting the data with a broken power-law with N_H fixed at the Galactic value. We find that the spectral index of the soft power-law is poorly constrained while the hard power-law has a spectral index $\alpha_x = 2.21 \pm 0.65$ (see Table 3). A two component model, consisting of a thermal component (black body, bremsstrahlung or Raymond-Smith dominating the soft part of the spectrum) plus a power-law does not yield a good fit of the data (P(χ^2) <0.01).

MS0144.2−0055 This source shows excess absorption relative to the Galactic value (see Figure 2c). The absorption excess in MS0144.2−0055 can be well parameterized by fitting the data with a power-law plus Galactic absorption plus a second absorption component (N_H=$1.5^{+0.8}_{-0.7} \times 10^{20}$ cm^{-2}) at the redshift of the source (see Table 3).

MS0310.4−5543 This source was included in the sample of 53 AGNs which exhibit ultra-soft X-ray excess (Ultra Soft Survey, USS) selected from *Einstein* IPC sources (Cordova et al. 1992, Puchnarewicz et al. 1992). However, given the few net counts detected by *Einstein* ($\sim$ 40 net counts) only a limited spectral analysis was possible.

The ROSAT observation ($\sim$ 7700 net counts detected) gives the opportunity to study the X-ray spectrum of this source in more detail. As shown in Figure 2d, the ROSAT data show a soft emission excess relative to a single power-law with N_H=$N_{H_{Gal}}$. We find that the soft excess in this source is well parameterized by fitting the data with a broken power-law with N_H fixed at the Galactic value. It gives $\alpha_{SOFT} = 3.89 \pm 1.09$, $\alpha_{HARD} = 1.54 \pm 0.13$, $E_{break} = 0.25 \pm 0.13$ keV and χ^2/dof=23.13/23 (see Table 3).

MS0919.9+4543 This source shows excess absorption relative to the Galactic value (see Figure 2e). As for MS0144.2−0055, also for this source the absorption excess can be well parameterized by fitting the data with a power-law including a Galactic absorption plus another absorption component (N_H=$2.7^{+1.6}_{-1.3} \times 10^{20}$ cm^{-2}) at the redshift of the source (see Table 3).

MS1215.9+3005 This source is the well know Seyfert 1 galaxy MKN 766. A detailed analysis of the ROSAT observations of this source is reported by Molendi, Maccacaro and Schaeidt (1993) and Molendi and Maccacaro (1994) while the results of the ASCA observation are reported by Leighly et al (1996). Its X-ray spectrum is very complicated, therefore we refer to these works for a detailed discussion of the X-ray properties of this source.

MS1747.2+6837 This is the Seyfert 1 galaxy Kaz 163. The ROSAT/PSPC data of this source were previously analyzed by Brandt et al. (1994). They find that a single power law model plus galactic absorption is not a good representation of the data since it would imply an N_H column density lower than Galactic value. However they showed that a broken power-law is a good representation of the spectrum, yielding $N_H=5.01^{+1.40}_{-1.27}\times10^{20}$ cm^{-2}, $\alpha_{SOFT}=2.59^{+0.81}_{-1.03}$, $\alpha_{HARD}=1.54^{+0.10}_{-0.10}$ with χ^2/dof=23.8/28.

In our analysis we confirm the results obtained by Brandt et al. (1994). However, since Brandt et al. (1994) showed that there are no indications of excess absorption ($N_H \sim N_{H_{Gal}}$) in the broken power-law model, we parameterized the soft excess fitting the data with a broken power-law fixing N_H at the Galactic value. With one less free parameter in the fit, we can better constrain the slopes of the broken power-law. We find $\alpha_{SOFT} = 2.93\pm0.50$ and $\alpha_{HARD} = 1.55\pm0.09$ (see Table 3).

MS2340.9−1511 This source shows a best fit value of N_H lower than the Galactic value, although only at the 68 per cent confidence level (see Figure 2f). Both the two power-law models with N_H fixed at the Galactic value and with N_H as a free parameter do not yield a good fit of the data ($P(\chi^2) \sim 1.5\times10^{-8}$ for both fits, see Table 2). We find that the X-ray spectrum of MS2340.9−1511 can be well fitted by a two component model consisting of a thermal component (kT=0.52±0.11 keV) based on the model calculations of Raymond and Smith (1977) with abundances fixed at the cosmic value, plus a power-law component ($\alpha = 2.06 \pm 0.07$). In table 3 we report the results for the Raymond-Smith + power-law fit. Other spectral models used to fit the data (broken power-law, black-body + power-law, bremsstrahlung + power-law) do not yield a good description of the data ($P(\chi^2)$ <0.01).

5.1.1 Warm Absorber

For the four sources that show a best fit value of N_H lower than Galactic value (MS0132.5− 4151, MS0310.4−5543, MS1747.2+6837, MS2340.9−1511 − MKN766 is not considered here for the reason stated above) we investigated the possibility that the soft excess could be a signature of an absorption produced not by neutral gas but by partially ionized "warm" material. A signature of such material is a flattening of the spectrum above the oxygen K-edge at $\sim$ 1 keV, and an excess flux below the edge, at $\sim$ 0.25 keV, where the ionized lighter elements become transparent. Given the limited spectral resolution of the ROSAT PSPC, warm absorbers could led to apparent soft excess in the X-ray spectra.

Fiore et al. (1996) have considered a number of warm absorber models and have computed for different values of the spectral index α_x, of the absorption column density N_H and of the ionization parameter U, the expected ratio of PSPC counts: R1 = (1.2−2.4 keV)/(0.6−1.0 keV) and R2 = (0.6−1.0 keV)/(0.2−0.4 keV). They have shown that "warm absorbers" cluster in a well define region of the R1 vs. R2 plane⋆.

We have computed the position of the four above mentioned sources in the R1 vs. R2 plane and discovered that all of them fall far away ($> 6\sigma$) from the "warm absorbers" region (see Figure 3). Therefore we can conclude that absorption by partially ionized "warm" material can be excluded for MS0132.5−4151, MS0310.4−5543, MS1747.2+6837 and MS2340.9−1511.

5.2 Analysis of the power-law spectral index

Within the general assumption that both the measurement errors and the underlying spectral index distributions can be described by a Gaussian, Maccacaro et al. (1988) used the Maximum-Likelihood (ML) analysis (see also Worrall and Wilkes 1990) to obtain the mean spectral index ($<\alpha_p>$) and the intrinsic spread in spectral slope (σ_p) of each class of extragalactic objects in the EMSS (we use here the same notation of Maccacaro et al. 1988, where the subscript "p" refers to the parent population). For the AGN sample they found an average spectral index $<\alpha_p>=1.03^{+0.05}_{-0.06}$ with an intrinsic dispersion σ_p=0.36.

In Figure 4 we show the distribution of the EMSS AGN energy spectral indices obtained from our analysis of the ROSAT data. Because a KS test shows that the spectral index distribution of the subsample of EMSS AGN used is not significantly different from a normal distribution (> 90 per cent confidence level), we used the ML analysis to calculate the mean ROSAT spectral index and the intrinsic dispersion.

Since at the time of the Maccacaro et al. (1988) analysis of the spectral properties of the EMSS AGN there was still a large number (236) of unidentified sources (of which 212 have since been identified) we have also repeated, for a more meaningful comparison, the ML analysis using the IPC data on the current (Maccacaro et al. 1994) EMSS AGN sample.

We have therefore considered 437 AGN (391 RQ and 46 RL) for the ML analysis, excluding 26 sources (23 RQ and 3 RL) for which the hardness ratio is so extreme to make the slope determination meaningless.

Table 4 and Figure 5 give the results of the ML analysis. In Table 4 we report the mean spectral index $<\alpha_p>$ and the intrinsic dispersion σ_p obtained with the ML analysis and, for comparison, the weighted mean $\overline{\alpha}_{\rm WM}$. Figure 5 shows the 90 per cent confidence contour for two interesting parameters for each data set (*Einstein*/IPC and ROSAT/PSPC).

A comparison of our IPC results on the whole EMSS AGN sample with the results obtained by Maccacaro et al. (1988), shows that we obtain the same mean spectral index with a small decrease in the intrinsic dispersion ($\Delta\sigma_p$=0.08). On the other hand, Table 4 and Figure 5 show that the mean PSPC spectral index is significantly steeper than the mean IPC spectral index ($\Delta\alpha \simeq 0.4$).

A similar discrepancy between IPC and PSPC slopes of AGN has been pointed out also by Laor et al. (1994) and Fiore et al. (1994). This difference is probably due to the "ultra-soft excess" below ∼0.3 keV first noted by Wilkes and Elvis (1987) in the IPC X-ray spectra of quasars and interpreted as the high-energy tail of the hot thermal component

⋆ Note that the label along X-axis of Figure 7 of Fiore et al. (1993) should read Counts(0.6−1.0) / Counts(0.2−0.4) and not Counts(0.2−0.4) / Counts(0.6−1.0) (Fiore, private communication)

dominating the UV emission (the big blue bump). Due to the softer ROSAT/PSPC band ($\sim 0.1-2.4$ keV) compared to the *Einstein*/IPC band ($\sim 0.3-3.5$ keV) the "ultra-soft excess" dominates in the ROSAT spectra and causes a steepening of the X-ray spectra when fitted with a single power-law. However, even if this "ultra-soft component" becomes dominant in the ROSAT band compared to the other components proposed to explain the X-ray emission above 0.5 keV (see Wilkes and Elvis 1987), we expect that its introduction causes a broadening in the spectral index distribution. In fact, because this thermal component comes from the inner accretion disk around the central black hole, different physical and/or geometrical properties of the latter may be responsible of different values of the observed spectral slope, with a consequent broadening of the spectral index distribution. The ML analysis shows (see Table 4 and Figure 5) that the intrinsic spread in the ROSAT spectral slopes is, in fact, greater than the intrinsic spread in the *Einstein* spectral slopes ($\Delta\sigma_p$=0.16). To ensure that this difference is not due to the different number of objects used (411 for IPC data and 55 for PSPC data), we repeated the ML analysis using only the IPC spectral indices of the 55 EMSS AGN that we used in our ROSAT analysis. For these sources we find $< \alpha_p >$=1.14 and σ_p=0.31. The ROSAT spectral indices show a greater intrinsic dispersion ($\Delta\sigma_p$=0.13) compared to the *Einstein* spectral indices also for the same data set. We therefore suggest that the difference between the ROSAT and *Einstein* spectral indices is due to the presence of the "ultra-soft excess" in the ROSAT/PSPC band. However, one should consider the possibility that up to 50% of this difference (*i.e.* $\Delta\alpha \lesssim 0.2$) may be due to calibration errors in the PSPC and/or IPC instruments. In fact, as suggested by Fiore et al. (1994) (see also Turner 1993), the maximum amplitude of the systematic error due to calibration is ~ 0.2 on the spectral index α_x.

Finally, considering only the ROSAT data, our values of the mean spectral index are consistent with previous values obtained for X-ray selected AGN. Using the CRSS sample, Ciliegi et al. (1996) find a mean spectral index $< \alpha_x >$=1.32 (σ_p=0.33) for the quasar sample and $< \alpha_x >$=1.30 (σ_p=0.49) for the NLXG sample, while Puchnarewicz et al. (1996) using the RIXOS AGN sample find $< \alpha_x >$=1.07 (σ=0.63). These mean spectral indices of X-ray selected AGN although marginally flatter, are also consistent with the values obtained for optically selected AGN. Laor et al. (1994) and Walter and Fink (1993) in fact, using samples of optically selected AGN, find a mean value of the ROSAT/PSPC spectral index of 1.50 ($\sigma = 0.40$ and $\sigma = 0.30$ respectively).

5.3 The radio-loud and the radio-quiet subsample

The spectral differences, in the X-ray band, between RL and RQ AGN have been studied by many authors. Wilkes and Elvis (1987) showed that RL objects have flatter X-ray spectra ($\alpha_x \sim$0.5 in the 0.3−3.5 keV band) compared to RQ objects ($\alpha_x \sim$1.0). Lawson et al. (1992), using EXOSAT data, showed that RL objects have X-ray spectral indices consistent with a single value (i.e. consistent with a dispersion σ=0.0), whereas RQ objects show a large spread in indices ($\sigma >$0.10).

Using the ML analysis we obtain the mean spectral index and the intrinsic dispersion for the RQ and RL EMSS AGN subsamples using the *Einstein*/IPC data (368 RQ and 43 RL) and the ROSAT data (50 RQ). Given the small number (5) of ROSAT RL AGN that we have analyzed, we do not apply the ML analysis to this subsample but we obtain a mean spectral index simply with the weighted mean. Table 4 and Figure 6 give the results of the ML analysis. It is clear that the mean index for the RL sample is flatter than that for RQ, and further that this group of objects shows no intrinsic dispersion, i.e. they are compatible (> 90 per cent confidence level) with a single spectral index, whereas there is an intrinsic dispersion present among the RQ samples (both from *Einstein* and ROSAT data). The same results were obtained by Lawson et al. (1992) with the EXOSAT data for a sample of 13 RQ and 18 RL quasars.

The flatter and possibly unique X-ray spectral index that we find also for the EMSS RL AGN with the IPC data, strengthen the scheme (Zamorani et al. 1981, Wilkes and Elvis 1987, Shastri 1991, Lawson et al. 1992) in which there is an additional component present in radio-loud objects which produces this single dominant power-law. This could be associated with beaming and jets present in many radio-loud quasar, as recently discussed by Kembhavi (1993) and Ciliegi et al. (1995).

Finally, Table 4 shows that also in the ROSAT data the RL sample shows a flatter spectral index than the RQ sample ($\Delta\overline{\alpha}_{\rm WM} = 0.42$). It thus seems that the additional X-ray component in the RL AGN dominates the X-ray spectra of these sources over almost two decades of energy ($\sim 0.1-10$ keV).

5.4 Correlation analysis

In this section we describe the search for correlations between α_x and other physical parameters, in particular redshift, optical and X-ray luminosity ($L_{2500\mathring{A}}$ and L_x) and optical to X-ray luminosity ratio ($L_{2500\mathring{A}}/L_x$).

The significance of the correlations is tested using the Spearman Rank correlation coefficient r_S and the relative probability P_r that an observed correlation could occur by chance for uncorrelated data sets (see Press et al. 1992). A correlation is taken to be significant when $P_r \leq 0.01$. A summary of all the correlation coefficients and their significance is given in Table 4, while Figure 7 shows redshift (z), optical luminosity ($L_{2500\mathring{A}}$), X-ray luminosity (L_x) and $L_{2500\mathring{A}}/L_x$, respectively, as a function of the X-ray energy spectral index α_x.

Given the hidden dependence of the normalization at 2 keV on the spectral slope α_x obtained from PSPC spectra (see Ulrich and Molendi 1995 for a detailed discussion of this point), we use, in the correlation analysis the broad band (0.1−2.4 keV) X-ray luminosity (L_x) which is much less sensitive to changes in α_x. For this reason we do not use the usual two point spectral index α_{ox} but instead we use the ratio between the optical (at 2500Å) and broad band X-ray luminosities ($L_{2500\mathring{A}}/L_x$).

Table 4 shows that no significant correlations are found. The lack of correlation between α_x and z for the EMSS AGN suggests that for these sources the power-law spectrum in the source rest frame extends from the soft ($\sim 0.1-2.4$ keV) into the hard X-ray band ($\sim 0.3-7.0$ keV for the highest

redshift object). Similar results are obtained for X-ray selected quasars by Ciliegi et al. (1996) and by Puchnarewicz et al. (1996) and for optically selected quasars by Canizares and White (1989) using *Einstein*/IPC data and by Williams et al. (1992) using Ginga data.

These results appear to be at odd with the result obtained by Schartel et al. (1992). Using the RASS data for 162 strongly-detected optically-selected QSOs Schartel et al. (1992) find a flattening of the spectral slope with increasing redshift from $\alpha_x \sim 1.5$ to $\alpha_x \sim 0.8$ between $z = 0.2$ and $z \sim 2$. The fact that both the EMSS and CRSS sample do not show any correlation between spectral index and redshift strengthen the suspect that the correlation observed in the Schartel et al. 1992 sample is spurious and due to an increasing fraction of RL AGN (that show flatter spectra) at high redshift. In fact, unlike the analysis carried out for the ROSAT spectra of the EMSS and CRSS sample, Schartel et al. (1992) did not make the important distinction between RL and RQ objects. Indeed the Ginga data appear to show a flattening of α_x with redshift but the correlation disappears when RL and RQ objects are considered separately (Williams et al. 1992).

Finally, the lack of a correlation between α_x and optical and X-ray luminosities is in agreement with the results obtained by Ciliegi et al. (1996) for the CRSS AGN and by Laor et al. (1996) for 23 QSOs of the Bright QSO Survey (BQS).

6 CONCLUSION

Using ROSAT/PSPC observations in the public archive (as of May 31, 1995) we have analyzed the X-ray spectra of 63 EMSS AGN. These objects are all the EMSS AGN detected by ROSAT with more than 300 net counts. A comparison with the whole sample of EMSS AGN shows that this subsample is not significantly different (redshift and luminosities distributions) from the whole EMSS AGN sample. This allows us to compare the PSPC results with the mean IPC spectral properties of the whole EMSS AGN sample. Our major results are the following:

1. Of the 42 sources with more than 600 net counts for which a detailed analysis was possible, eight (∼20 per cent) show a significant deviation from a single power-law model plus Galactic absorption. These eight sources were excluded from the sample used to study the mean X-ray spectral properties of the EMSS sources. Five of these sources show a soft emission excess relative to a single power-law fit with $N_H = N_{H_{Gal}}$ whereas the other three show a significant absorption excess ($N_H > N_{H_{Gal}}$). Using a color-color diagram developed by Fiore et al. (1993) we can exclude the possibility that the soft emission excess is due to absorption by partially ionized "warm" material.

2. The mean ROSAT/PSPC energy spectral index obtained with the Maximum-Likelihood analysis is $< \alpha_p > = 1.42$ with an intrinsic dispersion $\sigma_p = 0.44$. This value is in agreement with the ROSAT spectral indices obtained for other X-ray and optically selected AGN, and is significantly steeper ($\Delta\alpha \simeq 0.4$) than the mean *Einstein*/IPC spectral index obtained on the whole sample of EMSS AGN. Moreover we find a significant increase in the intrinsic dispersion of the ROSAT spectral indices compared to the *Einstein* data ($\Delta\sigma_p = 0.16$). The steepening of the ROSAT mean spectral index is probably due to the fact that in the ROSAT band (softer than the IPC band) the "ultra-soft excess", already noted in the spectra of many AGN below ∼0.3 keV, becomes dominant. In this scheme, the broadening of the ROSAT spectral index distribution can be explained considering that the slope of the ultra-soft component may differ from object to object, reflecting different physical and/or geometrical properties of the inner accretion disk with which it is associated.

3. The ML analysis of the IPC spectral index for RQ and RL EMSS AGN subsamples shows that the mean index of RL sample is flatter than that of the RQ. Moreover, as already obtained by Lawson et al. (1992) with the EXOSAT data, the RL sample has a 90 per cent confidence contour consistent with zero intrinsic dispersion (*i.e* compatible with an unique spectral index) whereas there is surely an intrinsic dispersion present in the RQ sample. These results support a scheme where in radio-loud objects there is an additional X-ray component characterized by a single dominant power-law.

4. Although we have ROSAT data for only 5 RL EMSS AGN, we find that also in the ROSAT band the mean index of RL is flatter than that of RQ. This suggests that the additional component in RL AGN dominates the X-ray spectra of RL AGN over almost two decades of energy ($\sim 0.1 - 10$ keV).

5. We found no significant correlation between the spectral index α_x and other physical parameters such redshift, optical and X-ray luminosity and the ratio between optical and X-ray luminosities. Similar results were obtained for other X-ray selected sample of AGN

ACKNOWLEDGMENTS

We thank R. Della Ceca, S. Molendi, F. Fiore and A. Wolter for useful discussions. PC acknowledges the partial support and hospitality of the Smithsonian Astrophysical Observatory (SAO) where part of this work was carried out. PC also thanks M. Elvis and B. Wilkes for encouragements and useful discussion during his stay at SAO. This work has received partial financial support from the Agenzia Spaziale Italiana (ASI contract: 191/3 AXG)

REFERENCES

Bevington P.R. and Robinson D.K. 1992, Data Reduction and Error Analysis for the Physical Sciences. McGraw-Hill, New York.

Boyle B.J., McMahon R.G., Wilkes B.J. and Elvis M., 1995 a, MNRAS, 272, 462

Brandt W.N, Fabian A.C., Nandra K., Reynolds C.S. and Brinkmann W., 1994, MNRAS, 271, 958.

Canizares C.R., and White J.L., 1989, ApJ, 339, 27.

Ciliegi P., Elvis M., Wilkes B.J., Boyle B.J. and McMahon R.G, 1996, MNRAS, in press.

Ciliegi P., Elvis M., Wilkes B.J., Boyle B.J., McMahon R.G and Maccacaro T., 1995, MNRAS, 277, 1463.

Comastri A., Setti G., Zamorani G., Elvis M., Giommi P., Wilkes B.J. and McDowell J.C., 1992, ApJ, 384, 62.
Cordova F.A., Kartje J.F., Thompson Jr. R.J., Mason K.O., Puchnarewicz E.M. and Harnden Jr. F.R., 1992, ApJS, 81, 661.
Elvis M., Green R.F, Bechtold J., Schmidt M., Neugebauer G., Soifer B.T., Matthews K. and Fabbiano G., 1986, ApJ, 310, 291.
Fiore F., Elvis M., Mathur S., Wilkes B.J. and McDowell J., 1993, ApJ, 415, 129.
Fiore F., Elvis M., McDowell J., Siemiginowska A. and Wilkes B.J., 1994, ApJ, 431, 515.
Gioia I.M., Maccacaro T., Schild R.E., Giommi P. and Stocke J.T., 1986, ApJ, 307,497.
Gioia I.M., Maccacaro T., Schild R.E., Wolter A., Stocke J.T., Morris S.L., and Henry J.P., 1990, ApJS, 72, 567.
Halpern J.P., 1981, Ph.D. Thesis, Harvard University.
Hasinger G., 1992, MPE Report n. 235, p. 321.
Kembhavi A.K. 1993, MNRAS, 264, 683.
Kruper J.S., Urry C.M. and Canizares C.R., 1990, ApJS, 74, 347.
Laor A., Fiore F., Elvis M., Wilkes B.J. and McDowell J.C., 1996, ApJ, submitted.
Laor A., Fiore F., Elvis M., Wilkes B.J. and McDowell J.C., 1994, ApJ, 435, 611.
Lawson A.J., Turner M.J.L., Williams O.R., Stewart G.C., and Saxton R.D., 1992, MNRAS, 259, 743.
Leighly K.M., Mushotzky R.F., Yaqoob T., Kunieda H. and Edelson R., 1996, ApJ, in press.
Maccacaro T., Gioia I.M., Wolter A., Zamorani G., and Stocke J.T., 1988, ApJ, 326, 680.
Maccacaro T., Wolter A., McLean B., Gioia I.M., Stocke J.T., Della Ceca R., Burg R. and Faccini R., 1994, Astrophysical Letters and Communications, 29, 267.
Malaguti G, Bassani L. and Caroli E., 1994, ApJS, 94, 517.
Molendi S. and Maccacaro T., 1994, A&A, 291, 420.
Molendi S., Maccacaro T., and Schaeidt S., 1993, A&A, 271, 18.
Petre R., Mushotzky R.F., Krolik J.H. and Holt S.S., 1984, ApJ, 280, 499.
Press W.H., Teukolsky S.A., Vetterling W.T. and Flannery B.P., 1992, 1992, *Numerical Recipes, Second Edition*, Cambridge: Cambridge Univ. Press.
Puchnarewicz E.M., Mason K.O., Romero-Colmenero E., Carrera F.J., Hasinger G., McMahon R., Mittaz J.P.D., Page M.J. and Carballo R., 1996, MNRAS, in press.
Puchnarewicz E.M., Mason K.O., Cordova F.A., Kartje J., Branduardi-Raymont G., Mittaz J.P.D., Murdin P.G. and Allington-Smith J., 1992, MNRAS, 256, 589.
Reichert G.A., Mushotzky R.F., Petre R. and Holt S.S., 1985, ApJ, 296, 69.
Schartel N., Fink H., Brinkmann W., and Trümper J., 1992, MPE Report no. 235 1992, p. 195.
Shastri P., 1991, MNRAS, 249, 640.
Stocke J.T., Morris S.L., Gioia I.M., Maccacaro T., Schild R.E., Wolter A., Fleming T.A., and Henry J.P., 1991, ApJS, 76, 813.
Stocke J.T., Liebert J., Schild R., Gioia I.M. and Maccacaro T., 1984, Ap, 277, 43.
Trümper J., 1983, Adv. Space Res., 2, No.4 241.
Turner T.J., in "The 1st Annual ROSAT Science Symposium and Data Analysis", University of Maryland, November 8−10, 1993.
Turner T.J. and George I.M., 1992, OGIP *Calibration Memo.*
Turner T.J. and Pounds K.A., 1989, MNRAS, 240, 833.
Ulrich M.N. and Molendi S., 1995, ApJ, December 95, in press.
Walter R. and Fink H., 1993, A&A, 274, 105.
Wilkes B.J. and Elvis M., 1987, ApJ, 323, 243.
Williams O.R. et al., 1992, ApJ, 389, 157.
Worrall D.M., and Wilkes B.J., 1990, ApJ, 360, 396.
Zamorani G. et al., 1981, ApJ, 245, 357.

Figure Captions

Figure 1. Comparison between the spectral slope α determined from the source hardness ratio and from a detailed spectral analysis.

Figure 2. Confidence contours (68, 90 and 99 per cent) for the joint determination of the energy spectral index and equivalent hydrogen absorbing column N_H, for six of the eight sources that show significant deviation from a simple power-law fit plus Galactic absorption. The vertical line represents the Galactic N_H value (Stark et al. 1992)

Figure 3. Ratio of the counts in the energy intervals 1.2−2.4 keV and 0.6−1.0 keV as a function of the ratio in the intervals 0.6−1.0 keV and 0.2−0.4 keV for α=0.5, N_H=1.2×10^{22} cm^{-2} (*crosses*); α=0.7, N_H=1.2×10^{22} cm^{-2} (*filled squares*); α=0.7, N_H=1.5×10^{22} cm^{-2} (*open squares*) and α=0.9, N_H=1.2×10^{22} cm^{-2} (*open circles*). In all cases U is varied between 0.1 and 0.2 (adapted from Fiore et al. 1993). The points numbered one to four represent the EMSS AGN with a best fit value of N_H lower than Galactic value.

Figure 4. Distribution of the energy spectral indices obtained from the analysis of the ROSAT data. The Radio-loud objects are shaded.

Figure 5. 90 per cent confidence contours obtained with the Maximum-Likelihood analysis for the whole EMSS AGN sample with the *Einstein*/IPC data (dotted line) and for the subsample of 55 EMSS AGN with the ROSAT/PSPC data (solid line) (see §5.2 for more details).

Figure 6. As in Figure 5, for Radio-loud (RL) and Radio-quiet (RQ) AGN separately.

Figure 7. ROSAT X-ray spectral indices for Radio-quiet AGN (open squares) and for Radio-loud AGN (filled squares) versus: (a) Redshift, (b) optical luminosity at 2500Å, (c) X-ray broad band (0.1−2.4 keV) luminosity and (d) $L_{2500\mathrm{A}^{\circ}}/L_x$.

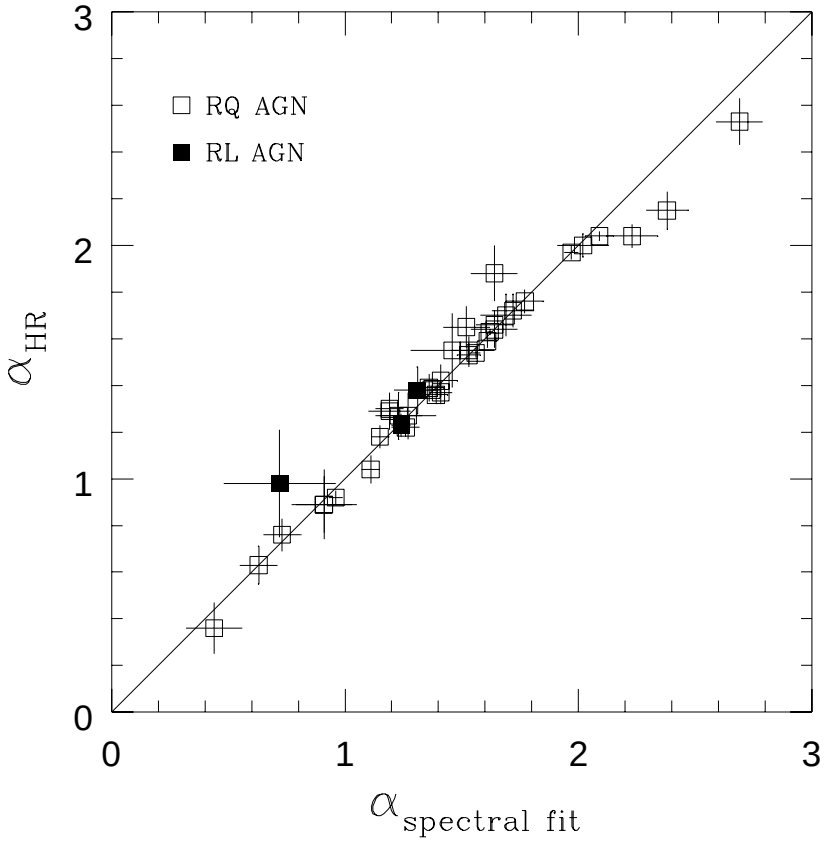
RQ AGN
RL AGN
$\alpha_{\rm HR}$
$\alpha_{\rm spectral\ fit}$
0
1
2
3

TABLE 1 : EMSS sources

SOURCE	NAME	z	α_{ro}	r ($\prime$)	θ ($\prime$)	Net Counts (0.1-2.4 keV)	Sequence Number
MS0017.3+1540		0.083	< 0.12	3.5	34.9	1177± 47	RP800253
MS0104.2+3153		2.027	< 0.20	3.2	15.7	1063± 81*	WP600106
MS0117.2−2837		0.347	< -0.01	4.0	29.9	1468± 43	RP700445
MS0120.0+0328		0.221	< 0.18	3.5	29.6	460± 34	WP701048
MS0132.5−4151		0.172		5.0	39.4	757± 44	RP700858
MS0144.2−0055		0.080	< 0.00	2.0	1.7	995± 33	WP701219
MS0204.8+0217		0.673	< 0.20	2.0	13.7	360± 23	RP700432
MS0232.5−0414	PKS	1.450	0.53	2.0	0.1	1490± 40	RP700350
MS0232.8−0400		0.376	< 0.13	3.0	15.4	773± 37	RP700350
MS0244.6−3020		0.530	< 0.12	2.5	8.6	507± 30	WP600449
MS0244.8+1928		0.176	< 0.08	4.0	32.6	1407± 43	RP700920
MS0310.4−5543		0.226		4.0	33.9	7709±105	WP701036
MS0439.7−4319	PKS	0.593	0.50	3.5	22.4	631± 39*	RP700867
MS0719.9+7100		0.125	< 0.08	5.0	31.4	900± 64	WP700210
MS0737.0+7436		0.312	< 0.16	2.5	15.5	1271± 39	RP800230
MS0803.3+7557		0.094	< 0.03	3.0	15.1	337± 22	WP700470
MS0828.7+6601		0.329	0.70	3.0	13.1	499± 52	RP800022
MS0828.7+6614		0.610	< 0.12	3.0	18.4	490± 49	RP800022
MS0832.6+6449		0.271	< 0.21	4.0	31.9	1138± 57	WP200654
MS0844.9+1836		0.086	< 0.07	3.5	30.7	493± 48*	WP800370
MS0845.1+3751		0.307	< 0.16	2.0	0.2	407± 30*	WP700546
MS0850.2+1336		0.194	< 0.15	4.0	27.4	1154± 46	RP700887
MS0919.3+5133		0.161	< 0.11	3.5	23.3	2393± 80*	WP600204
MS0919.9+4543		0.293	< 0.08	3.0	22.8	1606± 43	WP700539
MS1018.2+2010		0.250	< 0.23	2.0	18.0	584± 45*	RP200076
MS1059.0+7302		0.089	< 0.03	3.5	22.4	3464± 90*	RP700872
MS1112.5+4059		0.076	< 0.12	2.5	9.9	2347± 57	RP700855
MS1136.5+3413		0.032	< -0.02	3.5	22.8	890± 33	WP201120
MS1158.6−0323	MKN 1310	0.020	0.02	2.0	0.1	2414± 51	WP701202
MS1200.1−0330		0.065	0.12	3.5	26.1	1368± 60	WP201367
MS1214.3+3811		0.062	< 0.07	2.5	9.9	1327± 42	WP600179
MS1215.9+3005	MKN 766	0.013	0.11	3.0	13.5	65424±260	RP700970
MS1219.6+7535	MKN 205	0.071	−0.05	2.0	0.1	8651± 96	RP700434
MS1223.5+2522		0.067	< 0.04	2.0	9.7	745± 30	RP700388
MS1239.2+3219		0.053	< 0.09	4.0	29.9	799± 58*	RP600129
MS1248.0−0600		0.305	< 0.18	5.0	42.2	337± 26	RP600262
MS1248.7+5706		1.843	< 0.22	5.0	43.2	1018± 83	WP700208
MS1257.4+3439		1.375	0.28	4.0	29.7	781± 51	WP600164
MS1306.1−0115		0.111	< 0.17	5.0	42.6	547± 45	RP800248
MS1332.1+4138		0.311	< 0.13	4.0	26.0	1404± 55	RP800252
MS1335.1−3128		0.082	< 0.22	3.5	25.1	431± 54	RP600534
MS1342.8+6016		0.474	< 0.19	5.0	36.4	1283± 83	RP600270
MS1351.6+4005		0.062	< 0.05	4.0	29.0	790± 43	RP800485

TABLE 1 : Continued

SOURCE	NAME	z	α_{ro}	r ($\prime$)	θ ($\prime$)	Net Counts (0.1-2.4 keV)	Sequence Number
MS1408.1+2617		0.072	< 0.10	2.5	20.2	390± 29*	RP700359
MS1416.3−1257	PG 1416−12	0.129	< 0.01	2.0	0.1	3425± 66	WP700527
MS1426.5+0130	MKN 1383	0.086	-0.03	2.0	0.1	9697±105	RP150007
MS1549.8+2022		0.250	< 0.10	2.5	8.4	1535± 66*	WP701213
MS1559.1+3324		0.087	< 0.17	4.0	27.7	2510±102*	RP800003
MS1559.8+4202		0.759	< 0.10	3.5	24.6	342± 32	RP800103
MS1617.9+1731	MKN 877	0.116	< -0.04	2.0	0.1	1055± 33	RP700022
MS1640.0+3940		0.540	0.46	3.0	18.7	421± 35	RP700870
MS1703.7+2417		0.113	< 0.11	3.0	18.3	430± 27	RP400118
MS1746.2+6738		0.041	< 0.17	5.0	49.9	324± 24	WP700650
MS1747.2+6837	Kaz 163	0.063	< -0.01	2.0	10.6	6669± 84	WP701523
MS1803.6+6738		0.136	< -0.03	3.0	20.4	1255± 39	WP120013
MS2034.5−2253		0.256	< 0.08	2.0	1.0	529± 28	WP700547
MS2134.0+0028	PKS	1.936	0.84	2.0	3.0	433± 23	RP700817
MS2154.5+0107		0.220	< 0.16	3.0	15.7	309± 30	WP800344
MS2159.5−5713		0.083		3.0	14.3	3284± 65	RP200559
MS2254.9−3712		0.039	0.03	4.0	29.1	23145±165	RP600266
MS2255.0−3651		0.336	< 0.14	2.0	11.3	1636± 50	RP600266
MS2318.2−4220		0.212	< 0.16	5.0	34.6	428± 41	RP700333
MS2340.9−1511		0.137	< 0.01	2.0	0.7	12051±112	WP701205

* Normalized Net Counts. For this source an azimuthal sector centered on the source position has been excluded from the circle used for the counts extraction (see §3 for more details).

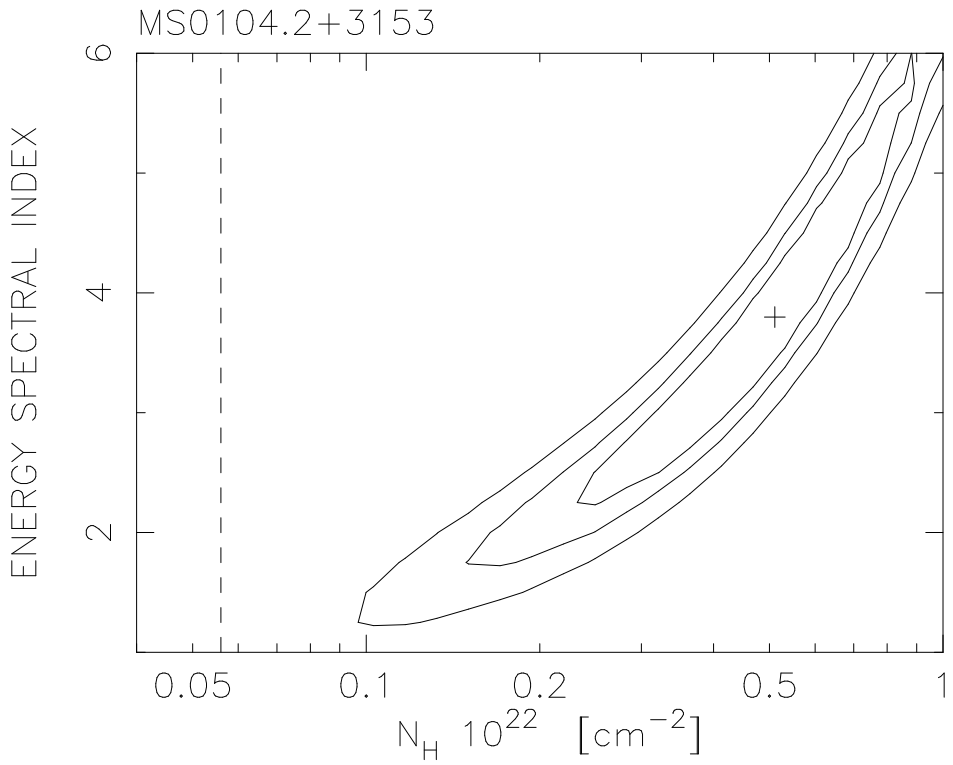
MS0104.2+3153
ENERGY SPECTRAL INDEX
2
4
6
0.05
0.1
0.2
0.5
1
N_H 10^22 [cm^-2]

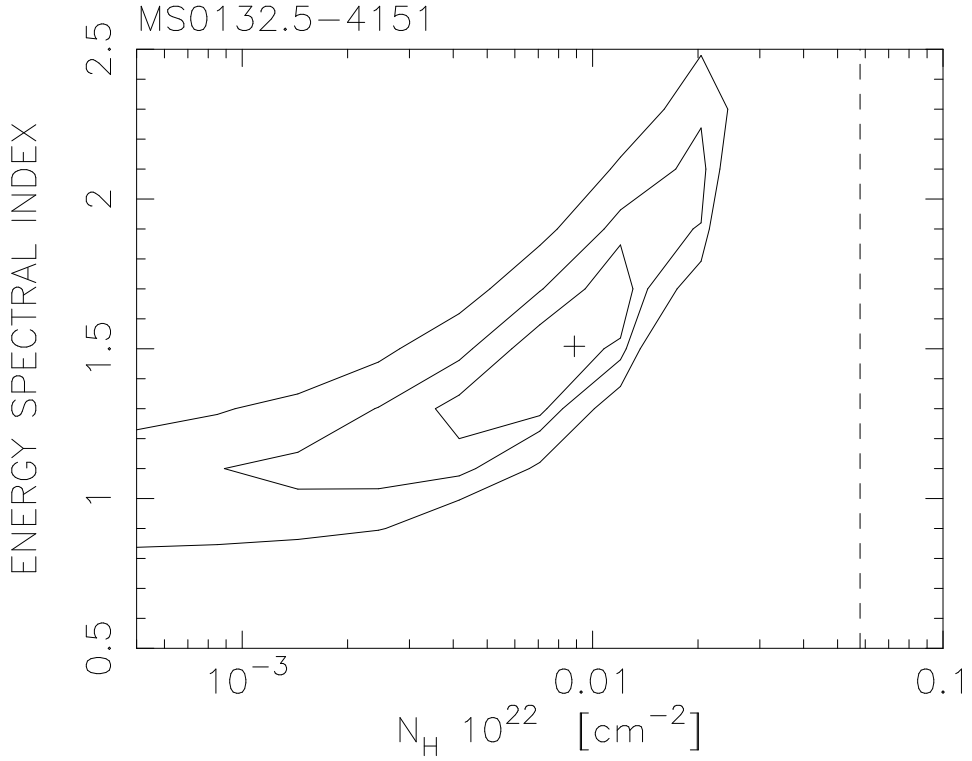
MS0132.5−4151
ENERGY SPECTRAL INDEX
0.5
1
1.5
2
2.5
10^{-3}
0.01
0.1
N_H 10^{22} [cm^{-2}]

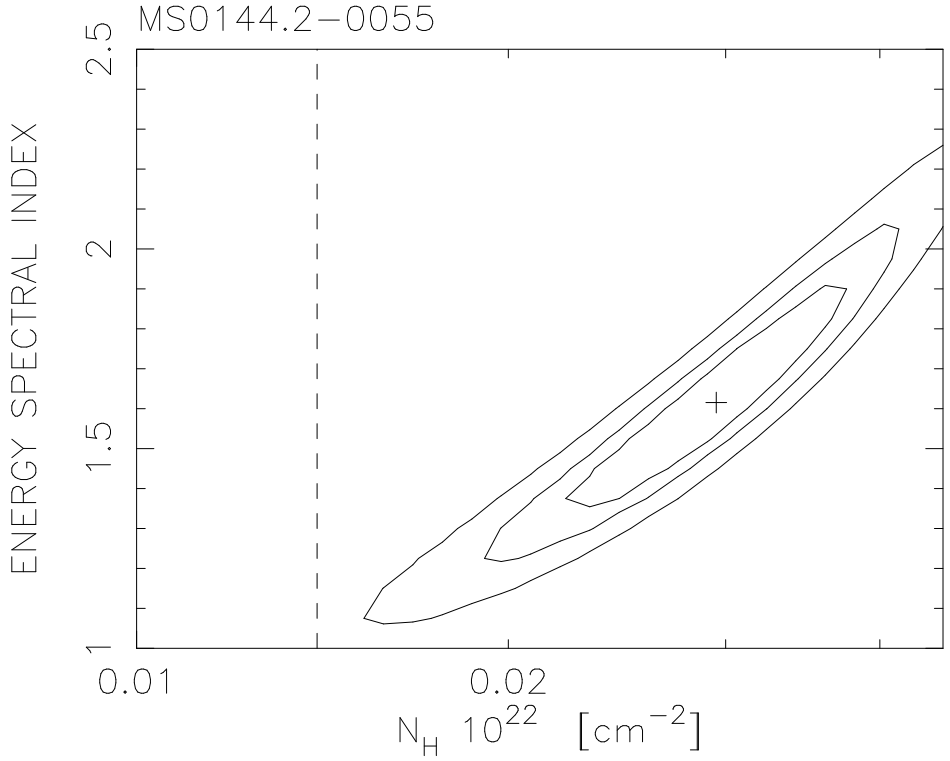
MS0144.2−0055
ENERGY SPECTRAL INDEX
2.5
2
1.5
1
0.01
0.02
N_H 10^22 [cm^−2]

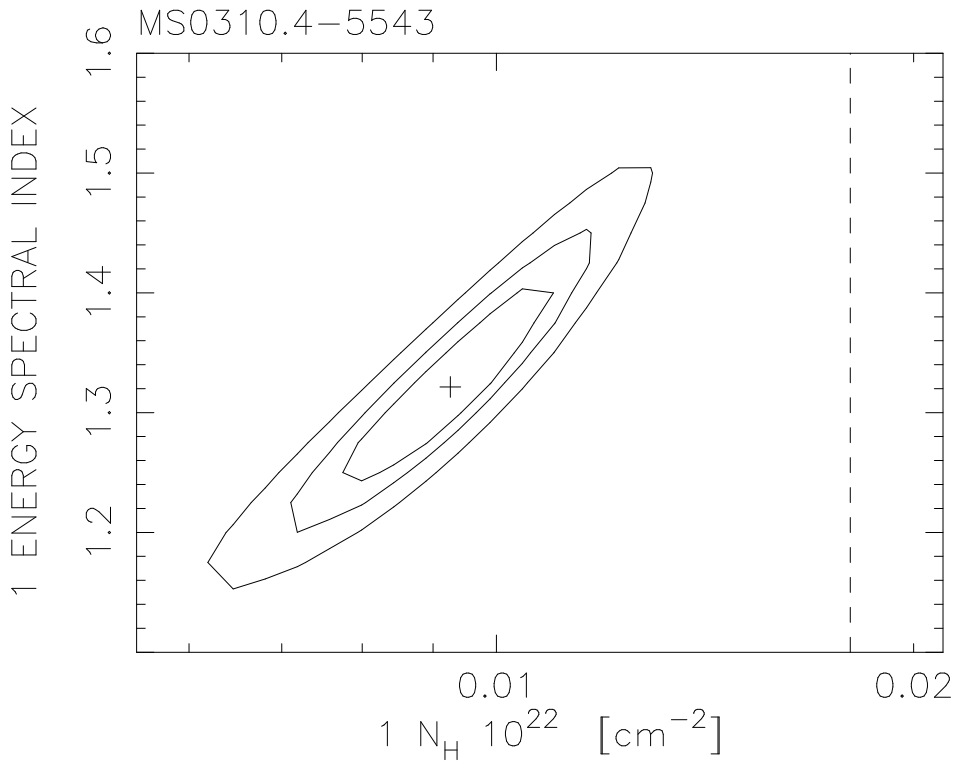
MS0310.4−5543
1 ENERGY SPECTRAL INDEX
1.2
1.3
1.4
1.5
1.6
0.01
0.02
1 N_H 10^22 [cm^-2]

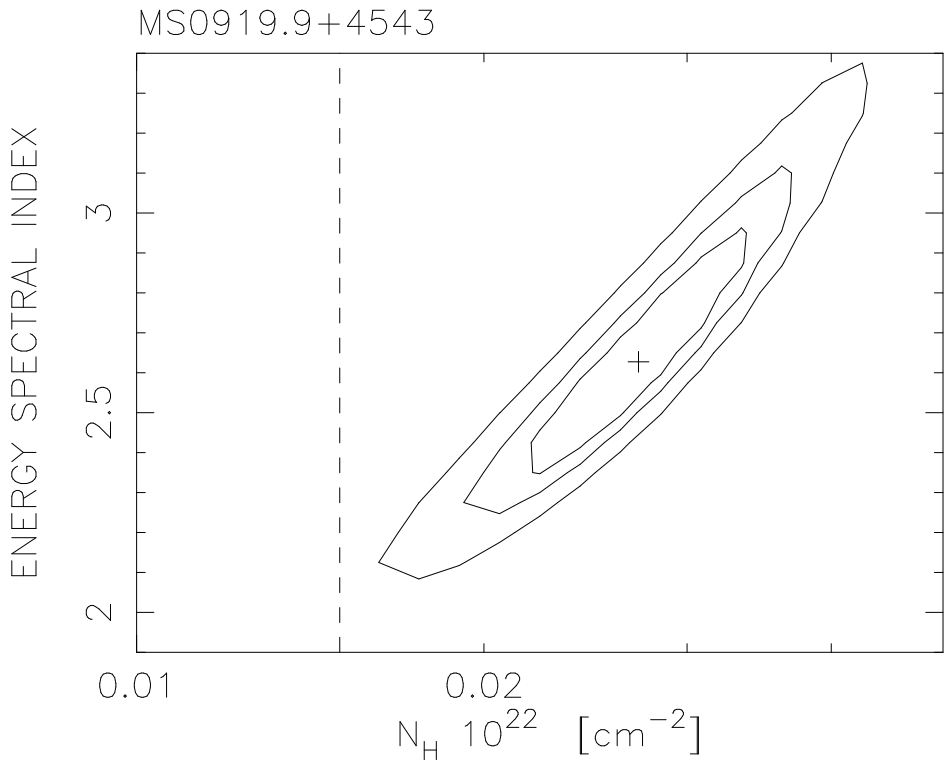
MS0919.9+4543
ENERGY SPECTRAL INDEX
2
2.5
3
0.01
0.02
N_H 10^22 [cm^-2]

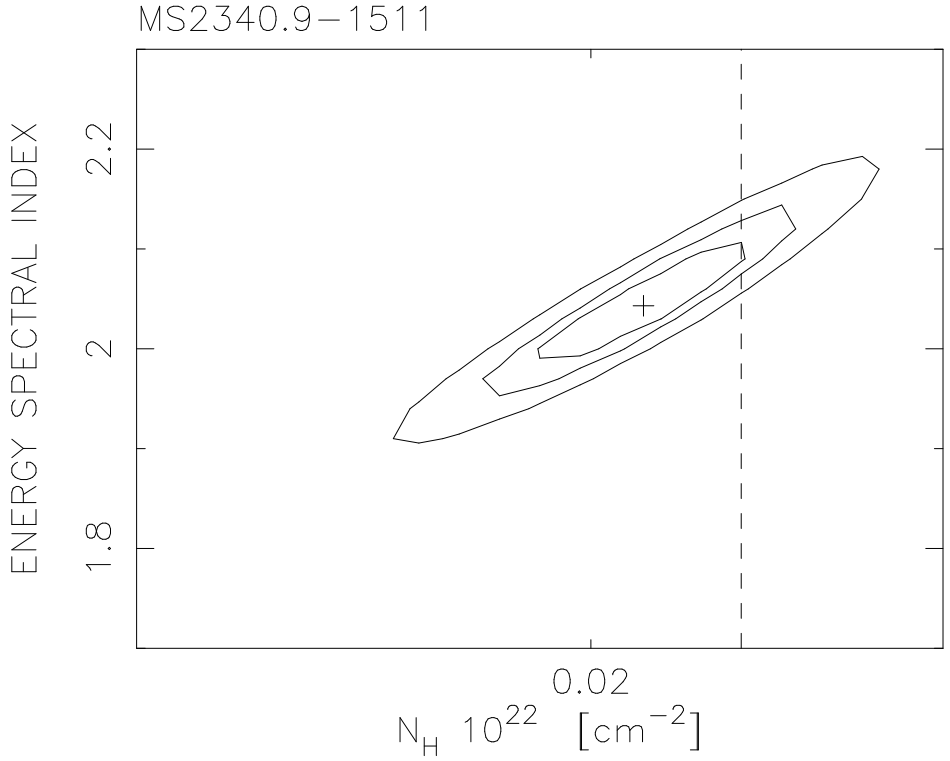
MS2340.9−1511
ENERGY SPECTRAL INDEX
2.2
2
1.8
0.02
N_H 10^{22} [cm^{-2}]

TABLE 2 : The X-ray spectral properties

	HR ANALYSIS		SPECTRAL ANALYSIS					
SOURCE	HR	α_{HR}	α_x	N_H ($\times10^{20}$ cm^{-2})	χ^2_{FIT}/dof	P($\chi^2 > \chi^2_{FIT}$)	P(F>F$_{FIT}$)	f_x^a
1	2	3	4	5	6	7	8	9
MS0017.3+1540	0.36±0.04	$1.42^{+0.07}_{-0.07}$	$1.41^{+0.07}_{-0.07}$	4.10	18.4/23	0.734		10.90±0.44
			$1.56^{+0.34}_{-0.33}$	4.60±1.10	17.9/22	0.713	0.420	
MS0104.2+3153	0.90±0.05	$0.85^{+0.37}_{-0.68}$	$0.83^{+0.15}_{-0.15}$	5.60	30.8/12	0.002		*
			$3.81^{+2.30}_{-1.63}$	51.1±35.6	11.9/11	0.374	0.001	
MS0117.2−2837	−0.78±0.02	$2.53^{+0.10}_{-0.09}$	$2.69^{+0.10}_{-0.10}$	1.70	13.3/13	0.422		90.01±2.63
			$2.96^{+0.41}_{-0.35}$	2.18±0.62	11.7/12	0.470	0.212	
MS0120.0+0328	0.06±0.06	$1.59^{+0.09}_{-0.09}$		3.20				11.40±0.79
MS0132.5−4151	−0.51±0.04	$3.56^{+0.11}_{-0.10}$	$3.61^{+0.17}_{-0.17}$	5.80	25.2/10	0.005		*
			$1.51^{+0.52}_{-0.40}$	0.89±0.81	5.1/9	0.825	2.2×10^{-4}	
MS0144.2−0055	−0.01±0.03	$0.99^{+0.04}_{-0.04}$	$1.01^{+0.05}_{-0.05}$	1.40	21.0/23	0.579		*
			$1.62^{+0.32}_{-0.30}$	2.95±0.82	9.9/22	0.987	5.4×10^{-5}	
MS0204.8+0217	−0.01±0.06	$1.70^{+0.09}_{-0.09}$		3.20				7.01±0.45
MS0232.5−0414 R	0.13±0.03	$1.23^{+0.05}_{-0.05}$	$1.24^{+0.04}_{-0.05}$	2.50	20.6/25	0.715		27.33±0.75
			$1.08^{+0.21}_{-0.19}$	2.09±0.50	19.2/24	0.742	0.203	
MS0232.8−0400	−0.39±0.04	$2.00^{+0.05}_{-0.07}$	$2.02^{+0.11}_{-0.11}$	2.50	10.9/13	0.617		21.10±1.02
			$1.82^{+0.32}_{-0.32}$	2.06±0.70	10.6/12	0.570	0.530	
MS0244.6−3020	−0.16±0.05	$1.41^{+0.08}_{-0.07}$		1.90				8.82±0.52
MS0244.8+1928	0.76±0.03	$1.88^{+0.12}_{-0.15}$	$1.64^{+0.10}_{-0.10}$	9.30	20.0/20	0.455		85.70±2.63
			$1.55^{+0.26}_{-0.25}$	8.60±1.60	19.6/19	0.418	0.531	
MS0310.4−5543	−0.40±0.01	$1.75^{+0.02}_{-0.02}$	$1.72^{+0.02}_{-0.02}$	1.80	85.9/25	1.3×10^{-8}		*
			$1.32^{+0.09}_{-0.08}$	0.93±0.17	44.3/24	0.007	7.9×10^{-5}	
MS0439.7−4319 R	0.06±0.07	$1.38^{+0.10}_{-0.11}$	$1.31^{+0.10}_{-0.10}$	2.50	15.9/14	0.322		12.12±1.43
			$1.38^{+0.50}_{-0.45}$	2.68±1.20	15.8/13	0.260	0.837	
MS0719.9+7100	0.07±0.06	$1.65^{+0.09}_{-0.09}$	$1.52^{+0.10}_{-0.10}$	3.40	9.6/13	0.726		14.90±1.07
			$1.54^{+0.57}_{-0.55}$	3.46±1.70	9.5/12	0.660	0.719	
MS0737.0+7436	0.22±0.03	$1.37^{+0.05}_{-0.05}$	$1.41^{+0.05}_{-0.05}$	3.30	16.6/24	0.866		38.13±1.19
			$1.65^{+0.30}_{-0.28}$	4.06±0.88	14.7/23	0.904	0.105	
MS0803.3+7557	0.18±0.06	$1.34^{+0.09}_{-0.09}$		3.00				20.50±1.37
MS0828.7+6601 R	0.59±0.10	$0.98^{+0.23}_{-0.27}$		4.20				2.74±0.29
MS0828.7+6614	0.31±0.09	$1.55^{+0.16}_{-0.16}$		4.20				4.26±0.43
MS0832.6+6449	0.65±0.06	$0.89^{+0.15}_{-0.18}$	$0.91^{+0.12}_{-0.12}$	4.40	12.4/18	0.823		10.15±0.51
			$0.99^{+0.36}_{-0.35}$	4.83±1.69	12.2/17	0.784	0.633	
MS0844.9+1836	0.30±0.09	$1.01^{+0.15}_{-0.15}$		2.70				5.69±0.55
MS0845.1+3751	−0.08±0.07	$1.77^{+0.11}_{-0.11}$		3.10				8.23±0.59

TABLE 2 : Continued

	HR ANALYSIS		SPECTRAL ANALYSIS					
SOURCE	HR	α_{HR}	α_x	N_H ($\times 10^{20}$ cm^{-2})	χ^2_{FIT}/dof	P($\chi^2 > \chi^2_{FIT}$)	P(F>F$_{FIT}$)	f_x^a
1	2	3	4	5	6	7	8	9
MS0850.2+1336	0.16±0.04	$1.55^{+0.06}_{-0.06}$	$1.53^{+0.07}_{-0.07}$	3.50	17.7/22	0.724		21.59±0.86
			$1.53^{+0.35}_{-0.33}$	3.51±1.00	17.7/21	0.668	1.000	
MS0919.3+5133	−0.67±0.02	$2.04^{+0.02}_{-0.02}$	$2.09^{+0.06}_{-0.06}$	1.40	18.1/18	0.452		31.47±1.05
			$2.60^{+0.32}_{-0.28}$	1.60±0.58	17.8/17	0.401	0.599	
MS0919.9+4543	−0.61±0.02	$2.01^{+0.02}_{-0.02}$	$2.04^{+0.06}_{-0.06}$	1.50	19.0/19	0.458		*
			$2.63^{+0.35}_{-0.30}$	2.72±0.67	7.3/18	0.987	4.2×10^{-5}	
MS1018.2+2010	−0.23±0.05	$1.72^{+0.07}_{-0.07}$		2.00				5.17±0.40
MS1059.0+7302	0.28±0.03	$1.18^{+0.05}_{-0.05}$	$1.15^{+0.04}_{-0.04}$	3.00	29.6/25	0.241		64.32±6.64
			$1.37^{+0.22}_{-0.22}$	3.67±0.64	26.9/24	0.311	0.144	
MS1112.5+4059	−0.28±0.02	$1.59^{+0.03}_{-0.03}$	$1.61^{+0.04}_{-0.05}$	1.90	15.9/24	0.892		25.53±0.62
			$1.43^{+0.20}_{-0.18}$	1.49±0.38	13.9/23	0.930	0.083	
MS1136.5+3413	−0.38±0.03	$1.76^{+0.05}_{-0.05}$	$1.77^{+0.08}_{-0.08}$	1.90	10.6/21	0.971		93.96±3.47
			$1.55^{+0.35}_{-0.31}$	1.44±0.63	9.5/20	0.924	0.184	
MS1158.6−0323	0.33±0.02	$0.92^{+0.03}_{-0.03}$	$0.96^{+0.03}_{-0.03}$	2.50	37.8/29	0.127		30.80±0.65
			$1.10^{+0.17}_{-0.17}$	2.94±0.47	35.7/28	0.152	0.203	
MS1200.1−0330	0.49±0.04	$0.63^{+0.08}_{-0.08}$	$0.63^{+0.08}_{-0.08}$	2.50	11.0/21	0.963		8.95±0.40
			$0.70^{+0.30}_{-0.30}$	2.77±1.08	10.8/20	0.951	0.604	
MS1214.3+3811	−0.03±0.03	$1.22^{+0.04}_{-0.04}$	$1.26^{+0.06}_{-0.06}$	1.90	16.2/29	0.973		16.20±0.52
			$1.57^{+0.15}_{-0.15}$	2.72±0.80	14.7/28	0.981	0.102	
MS1215.9+3005	−0.07±0.01	$1.16^{+0.01}_{-0.01}$	$1.19^{+0.01}_{-0.01}$	1.60	368/29	<0.001		*
			$1.42^{+0.03}_{-0.03}$	2.17±0.08	216/28	<0.001	1.3×10^{-4}	
MS1219.6+7535	0.20±0.01	$1.38^{+0.01}_{-0.02}$	$1.37^{+0.02}_{-0.02}$	3.20	30.9/29	0.372		290.5±3.24
			$1.39^{+0.08}_{-0.08}$	3.28±0.23	30.6/28	0.335	0.623	
MS1223.5+2522	−0.69±0.03	$2.15^{+0.08}_{-0.06}$	$2.38^{+0.09}_{-0.09}$	1.60	20.6/14	0.114		20.43±0.82
			$2.80^{+0.50}_{-0.40}$	2.46±0.90	17.5/13	0.177	0.157	
MS1239.2+3219	0.39±0.07	$0.36^{+0.11}_{-0.12}$	$0.44^{+0.12}_{-0.12}$	1.30	2.6/13	0.999		6.25±0.45
			$0.62^{+0.52}_{-0.48}$	1.85±1.50	2.3/12	0.999	0.186	
MS1248.0−0600	0.25±0.08	$0.89^{+0.12}_{-0.12}$		2.10				29.79±2.38
MS1248.7+5706	−0.24±0.06	$1.27^{+0.10}_{-0.10}$	$1.27^{+0.12}_{-0.12}$	1.30	20.6/7	0.004		8.32±0.68
			$0.77^{+0.57}_{-0.25}$	0.18±1.24	18.6/6	0.005	0.453	
MS1257.4+3439	−0.32±0.05	$1.29^{+0.08}_{-0.08}$	$1.19^{+0.09}_{-0.09}$	1.10	7.9/11	0.720		6.81±0.44
			$0.79^{+0.40}_{-0.29}$	0.30±0.53	5.4/10	0.864	0.060	
MS1306.1−0115	−0.23±0.07	$1.48^{+0.10}_{-0.11}$		1.80				10.20±0.84
MS1332.1+4138	−0.78±0.02	$2.04^{+0.05}_{-0.03}$	$2.23^{+0.11}_{-0.11}$	0.90	5.0/11	0.932		12.27±0.48
			$2.36^{+0.42}_{-0.34}$	1.05±0.53	4.6/10	0.914	0.410	
MS1335.1−3128	0.49±0.11	$1.14^{+0.21}_{-0.24}$		4.00				3.82±0.48
MS1342.8+6016	−0.31±0.05	$1.64^{+0.08}_{-0.08}$	$1.64^{+0.10}_{-0.10}$	1.90	6.5/12	0.888		8.97±0.59
			$1.32^{+0.50}_{-0.43}$	1.13±1.00	5.4/11	0.910	0.160	

TABLE 2 : Continued

	HR ANALYSIS		SPECTRAL ANALYSIS					
SOURCE	HR	α_{HR}	α_x	N_H ($\times 10^{20}$ cm^{-2})	χ^2_{FIT}/dof	P($\chi^2 > \chi^2_{FIT}$)	P(F>F$_{FIT}$)	f_x^a
1	2	3	4	5	6	7	8	9
MS1351.6+4005	0.01±0.05	$0.76^{+0.07}_{-0.07}$	$0.73^{+0.08}_{-0.08}$	1.00	20.0/18	0.340		7.98±0.44
			$1.15^{+0.41}_{-0.38}$	1.98±1.00	16.7/17	0.476	0.088	
MS1408.1+2617	−0.18±0.07	$1.27^{+0.10}_{-0.10}$		1.50				20.03±2.49
MS1416.3−1257	0.80±0.01	$1.04^{+0.06}_{-0.06}$	$1.11^{+0.04}_{-0.05}$	6.80	20.2/26	0.784		113.0±2.19
			$1.23^{+0.13}_{-0.14}$	7.52±0.70	17.6/25	0.859	0.068	
MS1426.5+0130	−0.03±0.01	$1.54^{+0.02}_{-0.02}$	$1.56^{+0.02}_{-0.02}$	2.70	30.9/29	0.371		325.0±3.55
			$1.50^{+0.08}_{-0.08}$	2.53±0.20	29.4/28	0.392	0.245	
MS1549.8+2022	0.18±0.04	$1.66^{+0.06}_{-0.06}$	$1.64^{+0.08}_{-0.08}$	3.90	14.7/20	0.794		32.86±1.41
			$1.59^{+0.41}_{-0.39}$	3.76±1.10	14.6/19	0.745	0.822	
MS1559.1+3324	−0.01±0.03	$1.36^{+0.04}_{-0.04}$	$1.39^{+0.05}_{-0.06}$	2.30	31.4/23	0.114		20.52±0.83
			$1.77^{+0.32}_{-0.30}$	3.35±0.90	27.4/22	0.197	0.087	
MS1559.8+4202	−0.69±0.07	$2.06^{+0.17}_{-0.06}$		1.40				5.97±0.57
MS1617.9+1731	0.46±0.03	$1.30^{+0.06}_{-0.06}$	$1.19^{+0.06}_{-0.06}$	4.00	34.1/26	0.134		45.96±1.44
			$1.01^{+0.21}_{-0.21}$	3.65±0.69	32.1/25	0.155	0.229	
MS1640.0+3940 R	−0.23±0.06	$1.11^{+0.09}_{-0.08}$		1.00				9.01±0.76
MS1703.7+2417	0.24±0.06	$1.73^{+0.10}_{-0.10}$		4.40				22.30±1.43
MS1746.2+6738	0.45±0.07	$1.32^{+0.13}_{-0.15}$		4.30				69.40±5.12
MS1747.2+6837	0.21±0.01	$1.82^{+0.02}_{-0.02}$	$1.80^{+0.02}_{-0.02}$	4.50	48.4/28	0.009		*
			$1.49^{+0.10}_{-0.10}$	3.54±0.29	25.4/27	0.550	3.6×10^{-5}	
MS1803.6+6738	0.48±0.03	$1.39^{+0.06}_{-0.06}$	$1.36^{+0.06}_{-0.06}$	4.70	16.0/25	0.916		84.89±2.64
			$1.31^{+0.26}_{-0.26}$	4.56±0.87	15.9/24	0.891	0.766	
MS2034.5−2253	0.52±0.05	$1.01^{+0.11}_{-0.11}$		3.80				9.49±0.50
MS2134.0+0028 R	0.85±0.04	$0.10^{+0.20}_{-0.24}$		4.40				15.70±0.85
MS2154.5+0107	0.75±0.10	$1.06^{+0.34}_{-0.50}$		6.10				7.14±0.71
MS2159.5−5713	−0.32±0.02	$1.97^{+0.03}_{-0.03}$	$1.97^{+0.03}_{-0.03}$	2.60	20.5/24	0.670		61.30±1.22
			$1.84^{+0.16}_{-0.17}$	2.28±0.40	19.0/23	0.702	0.194	
MS2254.9−3712	−0.49±0.01	$1.63^{+0.01}_{-0.01}$	$1.62^{+0.01}_{-0.01}$	1.20	39.7/29	0.090		112.4±0.80
			$1.53^{+0.05}_{-0.05}$	1.03±0.09	31.6/28	0.292	0.012	
MS2255.0−3651	−0.43±0.03	$1.53^{+0.05}_{-0.05}$	$1.53^{+0.05}_{-0.05}$	1.20	11.6/23	0.976		6.35±0.20
			$1.32^{+0.22}_{-0.19}$	0.80±0.37	9.3/22	0.991	0.031	
MS2318.2−4220	−0.46±0.06	$1.91^{+0.11}_{-0.11}$		1.90				15.70±1.53
MS2340.9−1511	−0.46±0.01	$2.03^{+0.01}_{-0.01}$	$2.10^{+0.02}_{-0.02}$	2.20	88.7/27	1.5×10^{-8}		*
			$2.04^{+0.08}_{-0.07}$	2.07±0.17	87.3/26	1.7×10^{-8}	0.523	

[a] Unabsorbed X-ray flux between 0.1-2.4 keV in unit of 10^{-13} erg cm^{-2} s^{-1}

∗ This source show a significant deviation from a single power-law plus Galactic absorption (see §5.1). Adequate spectral model and relative X-ray flux are reported in Table 3.

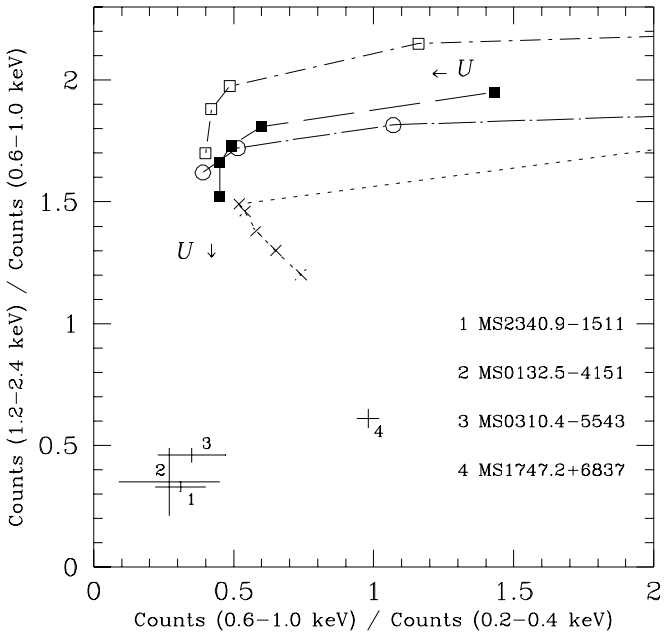
Counts (1.2−2.4 keV) / Counts (0.6−1.0 keV)
Counts (0.6−1.0 keV) / Counts (0.2−0.4 keV)
0
0.5
1
1.5
2
← U
U ↓
1 MS2340.9−1511
2 MS0132.5−4151
3 MS0310.4−5543
4 MS1747.2+6837
1
2
3
4

Table 3
Spectral models for the EMSS sources with a significant deviation from a power-law plus Galactic absorption.

Sources with "soft-excess"

SOURCE	Model	χ^2/dof	P($\chi^2 > \chi^2_{FIT}$)	E_{break} (keV)	α_{SOFT}	α_{HARD}	f_x^a
MS0132.5−4151	Broken power-law	10.97/8	0.203	0.32±0.10	5.00±2.64	2.21±0.65	350.0±18.23
MS0310.4−5543	Broken power-law	23.13/23	0.453	0.25±0.13	3.89±1.09	1.54±0.13	240.6± 3.30
MS1747.2+6837	Broken power-law	25.27/26	0.504	0.34±0.15	2.93±0.50	1.55±0.09	146.6± 1.85
SOURCE	Model	χ^2/dof	P($\chi^2 > \chi^2_{FIT}$)	kT (keV)	α_x		f_x^a
MS2340.9-1511	Power-law + Raymond-Smith	28.79/24	0.228	0.52±0.11	2.06±0.07		141.0± 1.31

Sources with "absorption excess"

SOURCE	Model	χ^2/dof	P($\chi^2 > \chi^2_{FIT}$)	N_H ($\times 10^{20}$cm^{-2})	z_{abs}	α_x	f_x^b
MS0104.2+3153	A : Power-law + Excess Absorption	11.80/11	0.379	47^{+44}_{-30}	0.111	$3.46^{+1.08}_{-1.05}$	5.4±0.30
MS0104.2+3153	B : Power-law + Excess Absorption	12.05/11	0.360	394^{+426}_{-258}	2.027	$2.98^{+0.90}_{-0.80}$	5.3±0.30
MS0144.2−0055	Power-law + Excess Absorption	9.86/22	0.988	$1.5^{+0.8}_{-0.7}$	0.080	$1.62^{+0.32}_{-0.30}$	18.7±0.62
MS0919.9+4543	Power-law + Excess Absorption	7.38/18	0.987	$2.7^{+1.6}_{-1.3}$	0.293	$2.70^{+0.40}_{-0.34}$	42.8±1.16

[a] Unabsorbed flux (0.1−2.4 keV) in unit of 10^{-13} erg cm^{-2} s^{-1}
[b] Unabsorbed (only for Galactic N_H) flux (0.1−2.4 keV) in unit of 10^{-13} erg cm^{-2} s^{-1}

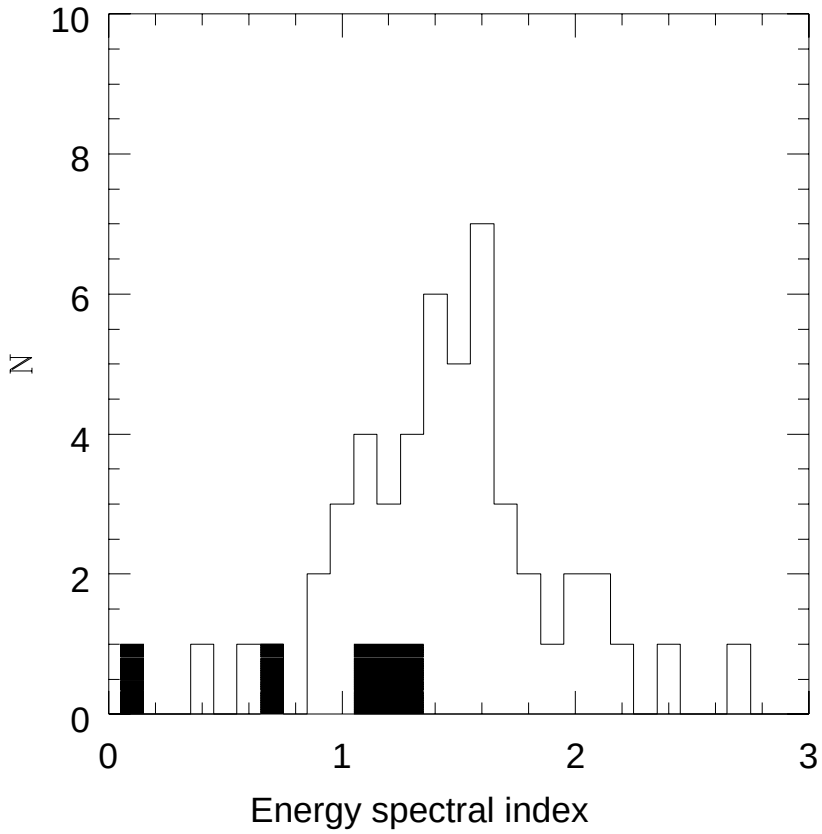
10
8
6
4
2
0
N
0
1
2
3
Energy spectral index

Table 4

Maximum Likelihood analysis and Weighted Mean X-ray spectral index

	Maximum Likelihood		Weighted Mean	Number Objects
Sample	$< \alpha_p >$	σ_p	$\overline{\alpha}_{\rm WM}$	
		***Einstein* IPC data**		
AGN (RQ + RL)	1.02	0.28	1.05	411
AGN RQ	1.04	0.28	1.08	368
AGN RL	0.81	0.11	0.78	43
		ROSAT PSPC data		
AGN (RQ + RL)	1.42	0.44	1.58	55
AGN RQ	1.47	0.42	1.59	50
AGN RL			1.17	5

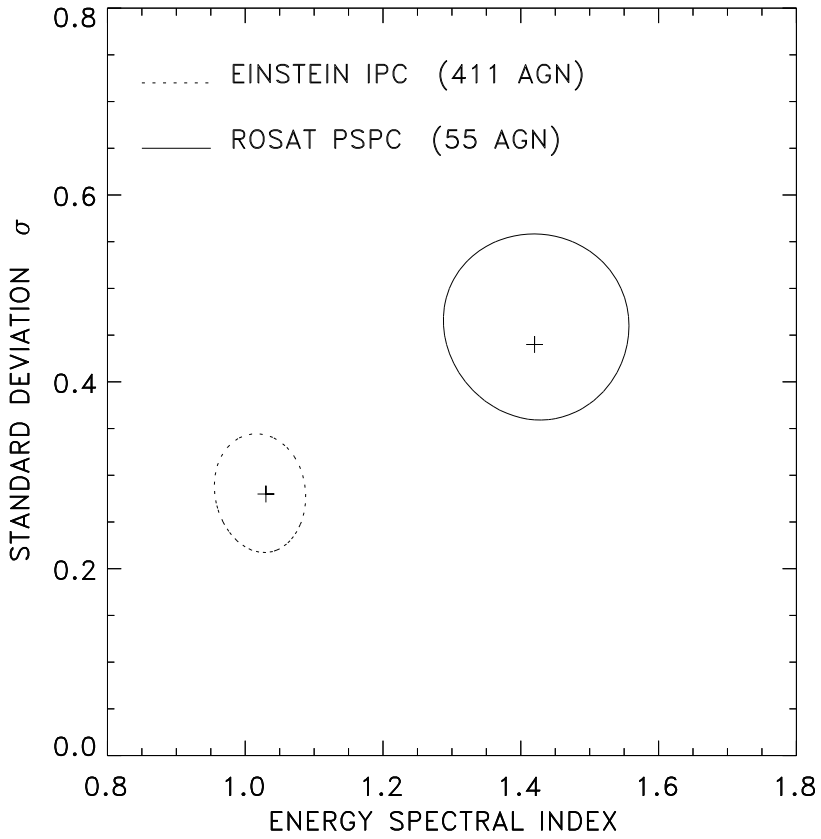
EINSTEIN IPC (411 AGN)
ROSAT PSPC (55 AGN)
STANDARD DEVIATION σ
0.0
0.2
0.4
0.6
0.8
0.8
1.0
1.2
1.4
1.6
1.8
ENERGY SPECTRAL INDEX

Table 5
Significance of Spearman Rank Correlation Analysis

Variables Correlated	Rs	P	d.o.f
AGN Radio Quiet			
α_x, z	0.281	0.048	48
α_x, L_x	0.324	0.022	48
α_x, $L_{2500\ \text{Å}}$	0.342	0.015	48
α_x, $L_{2500\ \text{Å}}/L_x$	−0.213	0.015	48
AGN Radio Loud			
α_x, z	−0.100	0.870	3
α_x, L_x	0.200	0.750	3
α_x, $L_{2500\ \text{Å}}$	−0.100	0.870	3
α_x, $L_{2500\ \text{Å}}/L_x$	0.700	0.190	3

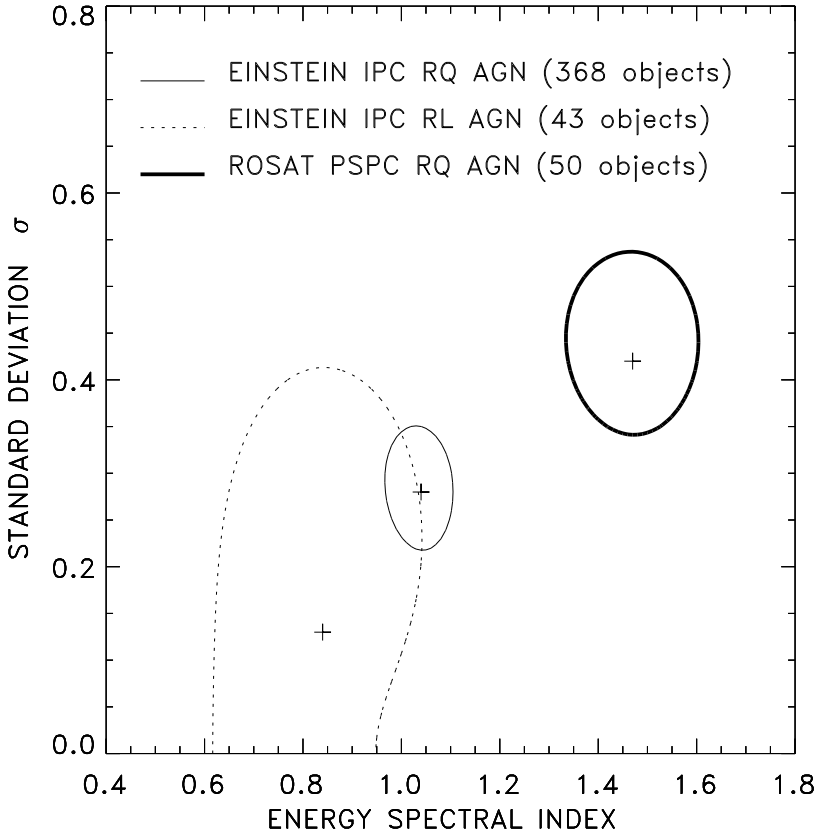
EINSTEIN IPC RQ AGN (368 objects)
EINSTEIN IPC RL AGN (43 objects)
ROSAT PSPC RQ AGN (50 objects)
STANDARD DEVIATION σ
ENERGY SPECTRAL INDEX
0.0
0.2
0.4
0.6
0.8
0.4
0.6
0.8
1.0
1.2
1.4
1.6
1.8

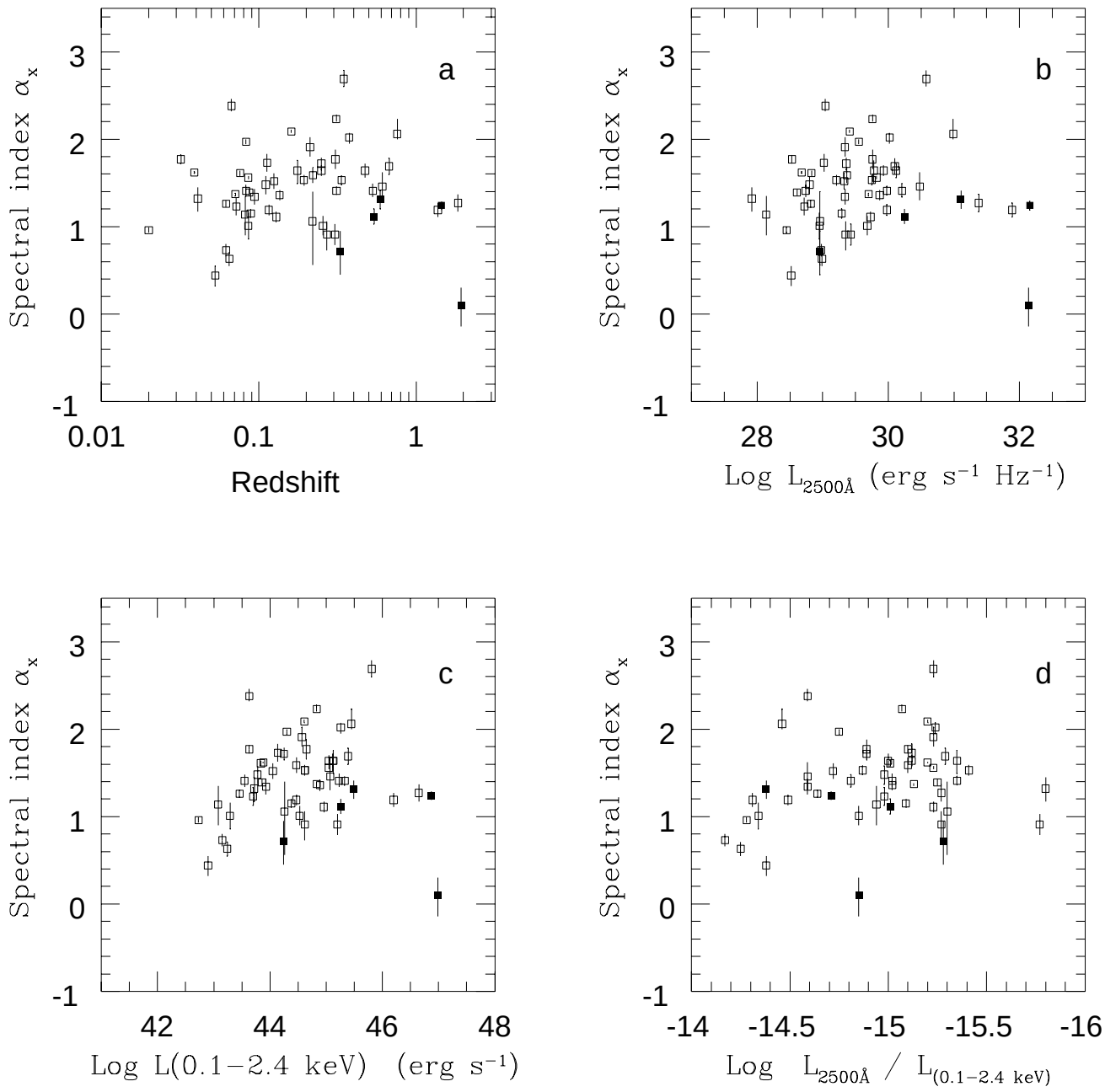
a
b
c
d
Spectral index α_x
Redshift
Log $L_{2500Å}$ (erg s^{-1} Hz^{-1})
Log L(0.1−2.4 keV) (erg s^{-1})
Log $L_{2500Å}$ / $L_{(0.1-2.4\ keV)}$